Investigation of Mechanical Properties and Optimization of Ultrasonic-Assisted Simple Shear Extrusion Process Using the Response Surface Method

Mostafa Balali[1], S.M. Hossein Seyedkashi[1*], Ali Hasanabadi[1], Hamid Gorji[2], Hamid Baseri[2], Mohammad Khosravi[3]

[1] Mechanical Engineering Department, University of Birjand, Birjand, Iran

[2] Mechanical Engineering Department, Babol Noshirvani University of Technology, Babol, Iran

[3] Mechanical and Materials Engineering Department, Birjand University of Technology, Birjand, Iran

[*] Corresponding author: seyedkashi@birjand.ac.ir

Abstract

This paper examines the mechanical performance and optimization of the Ultrasonic-Assisted Simple Shear Extrusion (USSE) process. Conventional severe plastic deformation (SPD) methods often suffer from high friction, elevated forming forces, and microstructural non-uniformity. However, the USSE method addresses these limitations by applying high-frequency ultrasonic vibrations. In this study, Finite Element Analysis (FEA) and the Response Surface Method (RSM) are used together to model the process and identify optimal operating conditions. Three main input parameters, punch speed, resonant frequency, and vibration amplitude, are evaluated for their influence on forming force and plastic strain. The findings indicate that vibration amplitude is the dominant factor, contributing 90.89% to forming force reduction and 82.41% to plastic strain enhancement. Increasing vibration amplitude and lowering punch speed effectively decrease forming force while promoting higher plastic strain. RSM optimization suggested the optimal conditions as a vibration amplitude of 30.11 μm, a punch speed of 0.61 mm/min, and a resonant frequency of 21.68 kHz. Under these conditions, the USSE process significantly reduced forming force and substantially increased plastic strain compared to the conventional SSE method. Surface roughness measurements showed that Specimen P4 exhibited 21%, 9%, and 6% lower roughness than P1, P2, and P3, respectively. Additionally, the optimized USSE sample demonstrated a 10% improvement in ultimate tensile strength and an 82% reduction in grain size relative to the SSE specimen. These outcomes confirm the effectiveness of the USSE technique and its superior mechanical and microstructural advantages.

keywords: Ultrasonic-assisted simple shear extrusion, finite element analysis, optimization, Mechanical properties, Microstructure.

1. Introduction

In the last few decades, various severe plastic deformation (SPD) techniques have been studied by a large number of researchers in order to achieve nanostructures and desired mechanical properties [1-3]. In the SPD processes, a large level of applied strain can be applied to the samples in the deformation zone in order to enhance their mechanical and microstructural properties [1]. One of the state-of-the-art SPD techniques is the simple shear extrusion (SSE) method, which was first introduced by Pardis and Ebrahimi [4]. However, challenges like high forming forces and microstructural heterogeneity limit their efficiency [5].To address these issues, applying high-frequency ultrasonic vibrations during SPD has gained attention due to the acoustic softening effect, which reduces flow stress and friction [6,7]. Zabihi et al. [8] showed that increasing the number of SSE passes on aluminum/alumina composites improves yield strength, hardness, and surface bonding. Sayari et al. [9] reported that SSE produces a more homogeneous fine-grain structure with higher shear strength in magnesium alloys compared to ECAP. Rezvani et al. [10] introduced circular SSE (CSSE), which reduces extrusion pressure and improves die efficiency relative to conventional SSE. Bagherpour et al. [11] found that nanostructured copper reaches maximum yield and tensile strength after eight SSE passes. The application of ultrasonic vibrations in SSE (USSE) significantly reduces forming force and friction [12, 13], a trend also observed when vibrations are applied to the punch in reverse extrusion [14]. Optimization studies of horn parameters in SSE indicated that horn and element type most strongly affect ultrasonic transmission and focusing efficiency [15]. In ECAP-based processes, ultrasonic assistance decreases forming force, increases microhardness [16], and improves plastic strain and structural homogeneity [17]. Zhilyaev et al. [18] showed that applying ultrasonic vibrations in ECAP increases the hardness and dislocation density of nickel alloy as the vibration amplitude rises. Rasooli et al. [19] found that ultrasonic vibrations improve the hardness, reduce surface roughness, and smooth the surface of aluminum alloys in rotational forming. Xie et al. [20] reported that higher vibration amplitude decreases friction and forming force while enhancing riveting quality. Ali et al. [21] demonstrated, using RSM and FE simulations, that simultaneous changes in triaxial stresses significantly affect soft fracture behavior in magnesium alloy during ECAP. Alateyah et al. [22] optimized parameters of coated pure copper using GA and RSM combined with FEA experiments. Ranjbari et al. [23] modeled vortex extrusion numerically and showed that force–angle interactions strongly influence material twisting under different friction conditions. Iqbal et al. [24] indicated that, among various parameters in twist extrusion, the number of passes has the greatest impact on tensile strength and microhardness. Overall, the main effect of ultrasonic vibrations in SPD processes is acoustic softening during application and acoustic hardening afterward, which transforms the crystal structure and increases yield strength [25]. Many studies have applied ultrasonic vibrations to the punch, but this approach can limit improvements in microhardness and microstructure [26].

However, a critical research gap remains: a comprehensive, systematic optimization of key USSE process parameters (vibration amplitude, punch speed, resonant frequency) and their interactive effects on critical outputs (forming force, plastic strain) is lacking. Previous studies have not fully leveraged integrated computational and statistical approaches for this purpose. Furthermore, recent advances in modeling and optimization of ultrasonic-assisted processes highlight the need for such an approach in USSE. Therefore, this study aims to bridge this gap by employing an integrated Finite Element Analysis (FEA) and Response Surface Methodology (RSM) approach to model, analyze, and optimize the USSE process. The specific objectives are to: (1) determine the individual and interactive effects of vibration amplitude, punch speed, and resonant frequency on forming force and plastic strain, and (2) identify the optimal parameter set that minimizes forming force while maximizing plastic strain.

The new proposed method that was reported as USSE by the authors [12, 13] applies ultrasonic vibrations in the SSE method. In this way, instead of applying ultrasonic vibrations to the punch, an area is created at the beginning of entering the deformation zone for the placement of the horn, so that commercial pure copper samples are passed through the deformation zone of the die, which applies a lot of applied strain to the samples by hitting this area while being vibrated. Figure 1 presents a general illustration of the mentioned process. Moreover, research on effective parameters and optimization of the combined USSE method can play a special role in increasing the efficiency of this process. Therefore, in addition to reporting the results from the FE simulation in the USSE method, the present study investigates effective input parameters, i.e. punch speed, resonant frequency, and vibration amplitude, to show the optimal values in the output parameters, i.e., forming force and plastic strain.

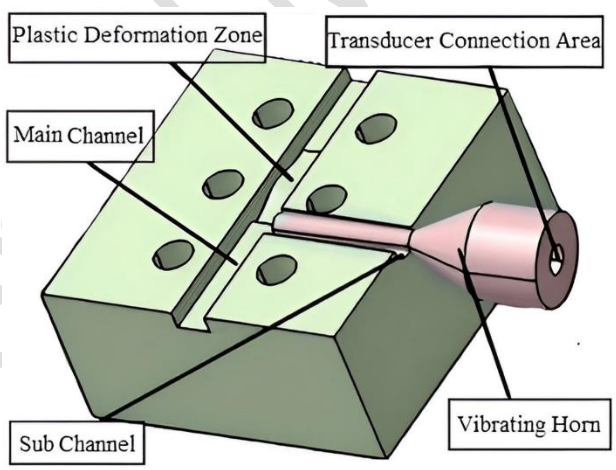

Figure 1. Schematic of Ultrasonic-Assisted Simple Shear Extrusion method (USSE)

2. Materials and Methods

2.1. Materials

The experimental samples used in this process were made of commercial pure copper, so that at first the samples were subjected to machining operations in order to reach the size of 14×14 mm^2

with 60 mm in length. Moreover, in order to avoid pre-heating during the extrusion process, the samples were annealed at a temperature of 650 °C for two hours and cooled inside the furnace. By applying ultrasonic vibrations to the samples and then extruding them, the mechanical and microstructural properties change under the two perspectives of acoustic softening and acoustic hardening, which will be discussed in more detail in the next section.

2.2. Design of Horn and die

The punch was made of SPK steel, while the steel die was made of Mo40. The ultrasonic vibrations were transmitted to the samples through the horn, which was placed at the beginning of entering the plastic deformation zone (PDZ). The samples were passed through the PDZ while contacting the vibrating horn. The horn material was chosen as the H13 steel due to its suitable mechanical and acoustic properties. A cylindrical-conical-cylindrical horn was used in order to amplify the vibration amplitude. The modal analysis and FE codes in the Abaqus software were used to design a suitable and accurate horn. In the modal analysis, in order to place the resonant frequency (f) of the horn in the frequency range of the booster (20 kHz), there was a need to change the dimensions of the designed horn, so that as the horn diameter and length decreased, the resonant frequency increased, and vice versa. A 20-kHz booster was used to provide the required amplitude amplification and to ensure proper impedance matching between the transducer and the horn. The ultrasonic system consists of a piezoelectric transducer, booster, and ultrasonic generator (pulser). The ultrasonic pulser/receiver used in the experiments was a Panametrics–Olympus 5077PR, a widely used and well-established system for industrial and laboratory ultrasonic testing applications. The piezoelectric transducer incorporates PZT-based ceramic elements with high electromechanical coupling efficiency, designed to operate at the nominal frequency of 20 kHz. The ultrasonic generator supplies a stable sinusoidal electrical signal at the same resonant frequency, with automatic frequency-tracking capability to compensate for load-dependent frequency shifts. This generator–transducer configuration ensures consistent vibration amplitude and stable power delivery throughout the forming process. Finally, the vibrating horn was designed according to the sub-channel of the USSE die. The ultrasonic horn employed in this study is a three-section cylindrical–conical–cylindrical design, selected to efficiently transmit and amplify longitudinal vibrations while maintaining structural stability during the process. A 20-kHz booster was used to provide the required amplitude amplification and to ensure proper impedance matching between the transducer and the horn. Also, in order to prevent the direct connection of the horn to the die, which increased the resonant frequency, the point where the vibration amplitude (a) was zero should be considered as a node. The horn was machined with high precision, followed by impedance-based tuning to match its natural frequency with the ultrasonic generator. The tip amplitude was calibrated using a laser vibrometer, confirming the experimental range of 5–30 µm. This design allows the ultrasonic vibrations to be applied directly at the entry of the shear deformation zone, improving energy-transfer efficiency compared with punch-based excitation and ensuring consistent and reproducible acoustic softening during the SSE process. These refinements provide a complete and reliable description of the horn configuration and justify the design choices for the USSE experiments. At this point, a flange was designed to be connected to the die. Figure 2 shows the horn design with longitudinal mode, resonant frequency of 20032 Hz, and flange area.

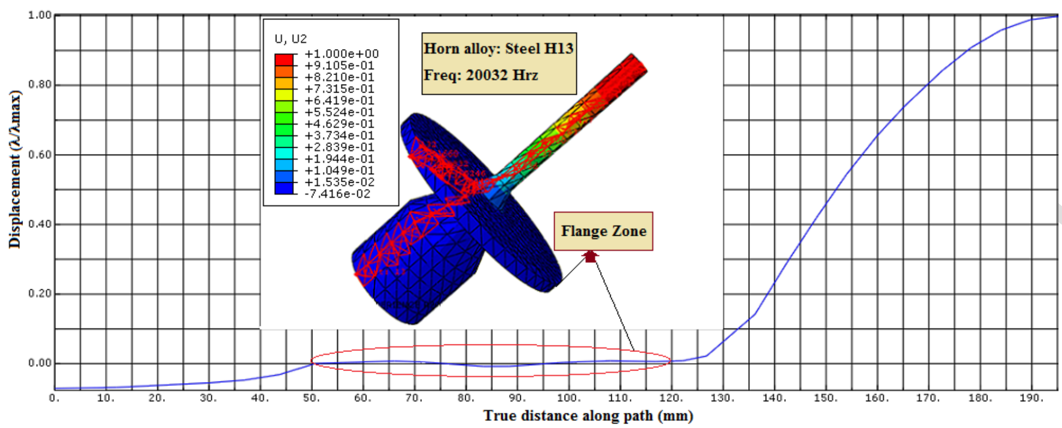

Figure 2. Oscillations range of the longitudinal mode and flange zone selection

After designing and manufacturing the horn, the vibration test was performed in order to obtain the resonant frequency of the horn. The vibration test results reported a resonant frequency of 20032 Hz, indicating an acceptable match with the resonant frequency of the horn designed through the modal analysis. In addition, the USSE die with a sub-channel, where the vibrating horn is placed, was manufactured as shown in Figure 3.

Figure 3. A view of the Ultrasonic-Assisted Simple Shear Extrusion die

2.3. Experiments

The die, punch, ultrasonic equipment, and vibrating horn are needed in order to conduct the USSE experiments. To this end, a 100-ton universal press machine with a punch speed (*V*) of 10 mm/min and a 2000-watt generator with a frequency of 5~70 kHz was used, as shown in Figure 4. The horn is placed on the secondary channel, which is perpendicular to the main channel of the die with a gap of 0.2 mm, and it is connected to the side wall of the die using a clamp. The samples enter the main die channel and are guided by the punch force to the vibrating area, which is located at the beginning of the deformation zone. While vibrating, they are passed through the PDZ area, which introduces a large applied strain to the samples. It is worth noting that by turning off the power generator, the USSE process becomes the SSE process. The observations confirmed that thermal softening plays only a minor role in the deformation process. The primary mechanism governing the enhanced plasticity and improved mechanical properties is athermal acoustic softening, which occurs during the application of ultrasonic vibrations. In this mechanism, ultrasonic energy interacts with dislocations and the crystal lattice, lowering the flow stress without significant heat generation. Although a slight temperature increase after vibration removal may contribute marginally to acoustic hardening, measurements showed that this effect is negligible compared to the dominant athermal response. Therefore, the improved deformability in the USSE process arises mainly from vibration-induced dislocation motion and lattice rearrangement rather than thermal effects.

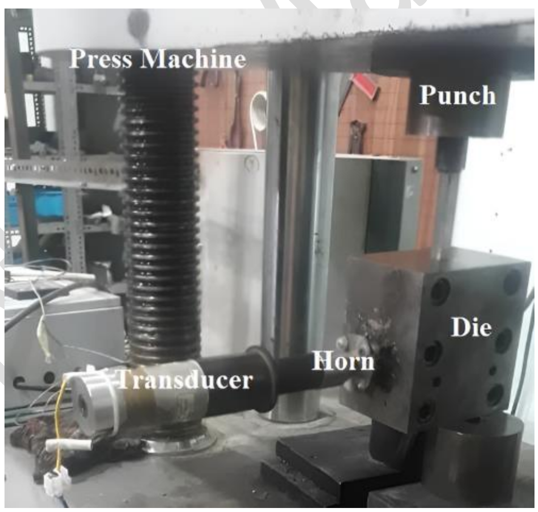

Figure 4. The USSE setup

The tensile tests were carried out by a 30-ton universal tensile machine (Zwick/Roell Z250). The extruded samples were first prepared according to the ASTM E8M standard, and then the tensile test was carried out with an initial load of 30 N/mm^2 and a speed of 1.5 mm/min for each sample. The microstructures of the samples were examined through a scanning electron microscope (SEM). In this test, first, the samples were sanded and polished with diamond paste in order to achieve a smooth and suitable surface. Finally, a suitable etching solution for the pure commercial copper samples was used with the combination of 25 ml H_2O + 5 ml HCl + 5 g F_eCl_3. Then, each sample was placed in the etchant for 15 seconds, and the microstructure was examined through the SEM. A surface roughness meter (Made: Taylor Hobson, Model: Surtronic 25) was used in order to obtain the surface roughness of the samples. Three points with a distance of 1.25 mm were considered on the central side surface of the samples for comparison.

2.4. Finite Element Analysis and Validation

The USSE process was modeled and simulated in the Abaqus/Explicit software and was compared with the experimental data in order to be validated. The extrusion punch and die were modeled as discrete rigid with R3D4 elements. The pure copper sample was modeled as a C3D8R element, and the elastic, plastic, and density properties were assigned to it. The important point about the USSE method was that in this method, the plastic properties (yield stress and plastic strain) were extracted from the tensile test and entered in the same way in the first pass of the simulation, and only the parameters, i.e. resonant frequency (f), vibration amplitude (a), and punch speed (V), were changed. The Dynamic/Explicit solver, as well as the Mass Scaling module, were used to reduce the processing time. In the USSE method, substantial deformation is introduced to the samples. The Finite Element Analysis (FEA) of the Ultrasonic-Assisted Simple Shear Extrusion (USSE) process was performed using an explicit solver to accurately capture the large plastic deformation and complex material flow induced by the combined effects of SSE and ultrasonic vibrations. To prevent excessive element distortion, the Arbitrary Lagrangian–Eulerian (ALE) adaptive meshing technique was employed, allowing the mesh to initially follow material deformation and subsequently remesh when necessary. During each remeshing cycle, material properties, including density, flow stress, and hardening behavior, were consistently transferred to the new mesh to ensure numerical continuity. The workpiece was discretized using structured hexahedral elements to improve the accuracy of shear-band and strain-gradient predictions. Mesh sensitivity analysis was conducted by refining the element size until the forming force and effective plastic strain converged within 2%. Mesh quality indicators (aspect ratio, skewness, and Jacobian values) were continuously monitored to maintain stability and accuracy. The final mesh provided adequate resolution in the deformation zone while keeping computational cost manageable. By integrating ALE with a rigorously validated mesh, the simulation reliably reproduced material flow, strain distribution, and forming forces in the USSE process, ensuring strong agreement with experimental observations. Finally, the process meshing was done using the Sweep technique with a global approximation of size 0.5 mm. Figure 5 shows the FE and meshed models.

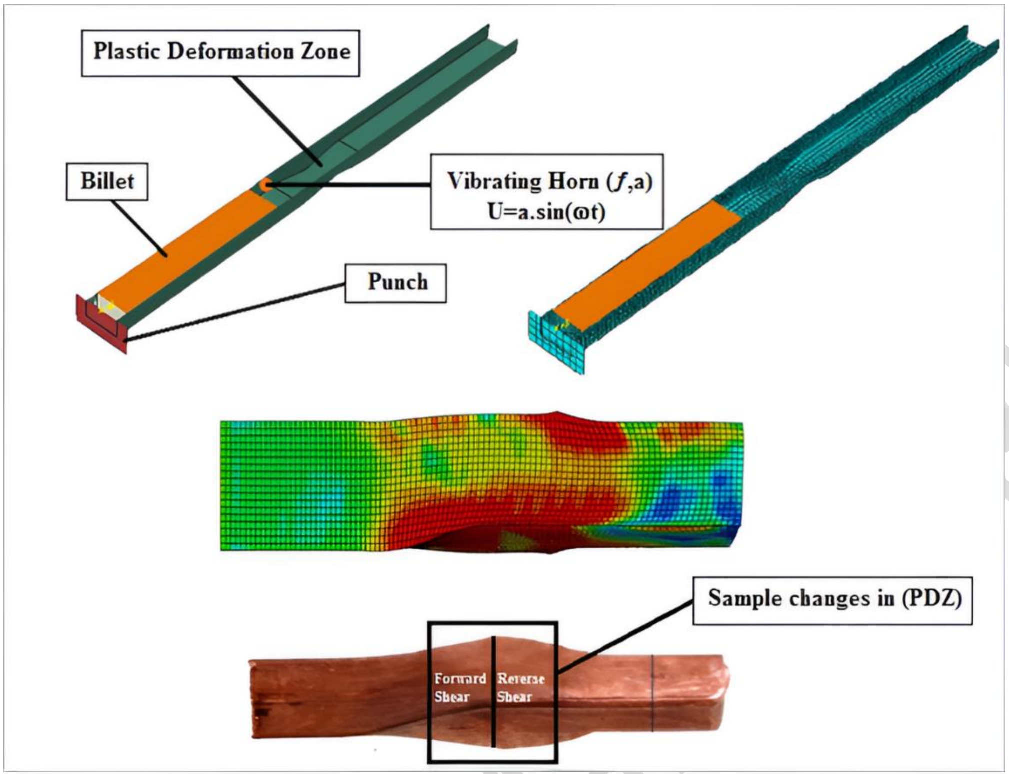

Figure 5. Finite element models and meshing in the USSE method

In order to validate the results from the FE simulation with the experimental results, the force-displacement curve was considered. Figure 6 shows the comparison of the FE and experimental results, presenting an error of 4.5%, which indicates an acceptable agreement between the results. To ensure a rigorous validation of the experimental and simulation results, the standard metrics of Root Mean Square Error (RMSE) and Mean Absolute Percentage Error (MAPE) were employed (Table 1). These metrics offer a quantitative and reproducible assessment of the deviations, effectively capturing both the global agreement and local point-to-point variations between the datasets. The detailed analysis yields an RMSE of 1.45 kN and a MAPE of 8.5%. The coefficient of determination (R^2) is a statistical measure (between 0 and 1) that indicates how well a model explains the variability (variance) in the observed data. The high R^2 value of approximately 0.96 indicates an excellent fit, confirming that the model explains 96% of the variance in the experimental data. These values confirm that the overall accuracy of the finite element model is within an acceptable range, thereby substantiating its reliability for the parametric study undertaken in this work.

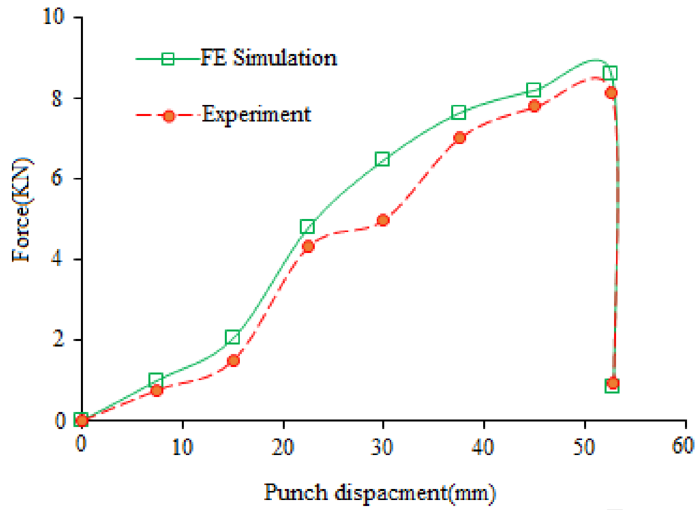

Figure 6. Comparison of experimental and FE force-displacement diagrams in the USSE method

Table. 1. Statistical validation metrics for the finite element model (RMSE, MAPE, and R^2)

Metric	Value	Explanation
RMSE	1.45 kN	Average absolute error between curves
MAPE	8.5%	Average relative error
R^2	≈ 0.96	Proportion of variance explained by the model

2.5. Response Surface Method

The RSM is one of the most efficient statistical methods for modeling and analysis of engineering processes. The present study uses a second-order polynomial regression model in order to obtain the output behavior based on the input parameters and provide the optimal points. In fact, the main aim of the design of experiments (DOE) methods is to model the process with the minimum number of experiments and an acceptable level of modeling error. In addition, the analysis of variance (ANOVA) is used to analyze the effects of input parameters on the outputs [27]. In the USSE process, the quality of the extruded samples is influenced by three input parameters, i.e. resonant frequency, vibration amplitude, and punch speed. Considering the acceptable results and good compatibility between the simulated and experimental samples, the FEM method was used to study the effects of these parameters on two output parameters (responses) of forming force (F) and plastic strain (ε). Table 2 shows the DOE table to be used in the FE simulations. The DOE was carried out using the central composite design (CCD) technique. The CCD method was chosen based on the value of α=1.682 for axial points, which creates five different levels for each parameter. So, 20 tests were determined.

Table. 2. Design of experiments for input parameters

Parameter	Symbol	Unit	-α	-1	0	+1	+α
Resonant frequency	f	kHz	18.3182	19	20	21	21.6818
Vibration amplitude	a	μm	4.8866	10	17.5	25	30.1134
Punch speed	V	mm/min	0.6137	3	6.5	10	12.3863

In this process, in order to achieve a reliability of 95%, the parameters with P-values greater than 0.05 are ignored, and only the values less than 0.05 are reported as significant parameters. Figure 7(a–b) presents the complete set of diagnostic residual plots for the two response variables Force and Plastic strain including the normal probability plot, residual histogram, residuals versus fitted values, and residuals versus observation order. Collectively, these plots demonstrate that the developed regression equations satisfy the fundamental assumptions required for statistical model adequacy. The normal probability plots show that the residual points for both responses lie closely along the reference line, with only minor deviations at the extremes. This indicates that the residuals are approximately normally distributed and that the normality assumption is not violated. The histograms likewise exhibit an almost symmetric, unimodal distribution centered around zero, with no evidence of skewness or abnormal tail behavior. The residuals versus fitted values plots display random scatter with no discernible pattern, confirming homoscedasticity and the appropriateness of the model's functional form. Similarly, the residuals plotted against observation order reveal no trend, cyclicity, or periodic behavior, confirming the independence of the error terms. Finally, the lack-of-fit test, with p-values exceeding 0.05 for both response variables, indicates that no significant lack-of-fit exists. Thus, the proposed polynomial regression model provides an adequate and reliable representation of the experimental data across the entire domain studied.

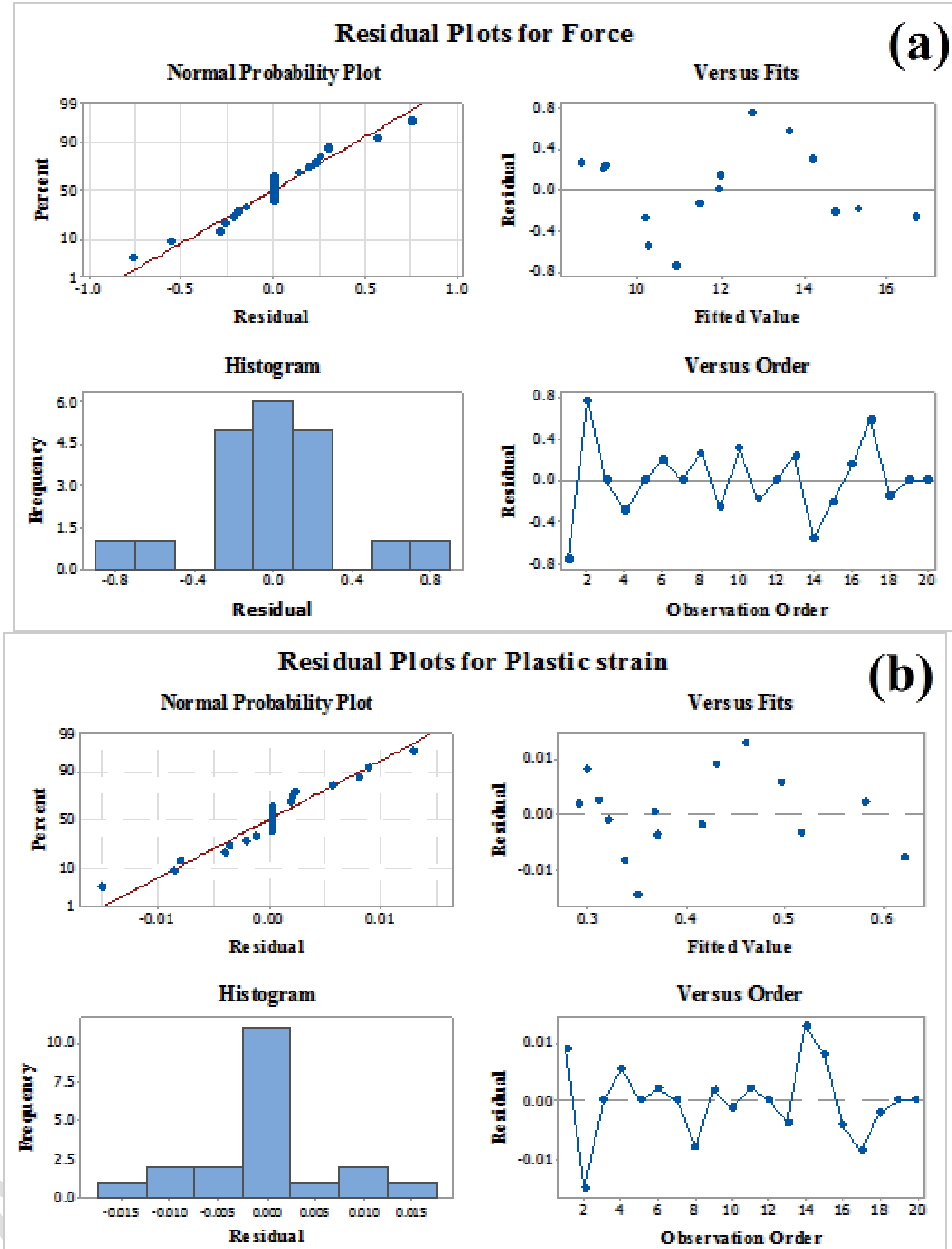

Figure 7. Residual plots for evaluating the adequacy of a) the forming force, b) plastic strain

3. Results and Discussion

3.1. Response Surface Modelling

The present study used the RSM and CCD in order to design the experiments for the input variables, i.e. the resonant frequency, the vibration amplitude, and the punch speed, along with their change interval in five levels. After designing twenty tests in the RSM, each test was simulated using FEA in Abaqus/Explicit software. Plastic strain and forming force were obtained as given in Table 3.

Table. 3. The responses obtained from FEA for the designed experiments

No	*f* (kHz)	*a* (μm)	*V* (mm/min)	F (kN)	ε
1	20.0000	17.5000	0.6137	10.163	0.438
2	20.0000	17.5000	12.3863	13.495	0.334
3	20.0000	17.5000	6.5000	11.947	0.367
4	21.0000	25.0000	10.0000	9.874	0.502
5	20.0000	17.5000	6.5000	11.947	0.367
6	21.0000	25.0000	3.0000	9.321	0.584
7	20.0000	17.5000	6.5000	11.947	0.367
8	20.0000	30.1134	6.5000	8.892	0.614
9	20.0000	4.8866	6.5000	16.418	0.291
10	19.0000	10.0000	3.0000	14.483	0.318
11	19.0000	10.0000	10.0000	15.109	0.312
12	20.0000	17.5000	6.5000	11.947	0.367
13	19.0000	25.0000	3.0000	9.435	0.513
14	19.0000	25.0000	10.0000	9.682	0.473
15	21.0000	10.0000	10.0000	14.541	0.306
16	18.3182	17.5000	6.5000	12.121	0.365
17	21.0000	10.0000	3.0000	14.208	0.328
18	21.6818	17.5000	6.5000	11.317	0.412
19	20.0000	17.5000	6.5000	11.947	0.367
20	20.0000	17.5000	6.5000	11.947	0.367

Based on the obtained responses, the ANOVA was used in Minitab software to determine the significant parameters and the contribution percentage of the input parameters. The ANOVA table for each of the forming force and plastic strain is presented in Tables 4 and 5, respectively. It should be noted that these tables present the final results in which the insignificant parameters are eliminated from the model.

Table. 4. The results of ANOVA for the forming force

Source	DF	Seq SS	Contribution	F-Value	P-Value
Model	3	83.2114	96.68%	155.20	0.000
Linear	2	82.2002	95.50%	229.97	0.000
a	1	78.2307	90.89%	437.74	0.000
V	1	3.9694	4.61%	22.21	0.000
Square	1	1.0113	1.17%	5.66	0.030
$a \times a$	1	1.0113	1.17%	5.66	0.030
Error	16	2.8595	3.32%		
Lack-of-Fit	11	2.8595	3.32%		
Pure Error	5	0.0000	0.00%		
Total	19	86.0709	100.00%		

Table. 5. The results of ANOVA for the plastic strain

Source	DF	Seq SS	Contribution	F-Value	P-Value
Model	9	0.161468	99.53%	237.56	0.000
Linear	3	0.143874	88.69%	635.02	0.000
f	1	0.002453	1.51%	32.49	0.000
a	1	0.133691	82.41%	1770.22	0.000
V	1	0.007730	4.76%	102.35	0.000
Square	3	0.014917	9.20%	65.84	0.000
$f \times f$	1	0.000398	0.25%	14.62	0.003
$a \times a$	1	0.013627	8.40%	187.90	0.000
$V \times V$	1	0.000892	0.55%	11.81	0.006
2-Way Interaction	3	0.002677	1.65%	11.82	0.001
$f \times a$	1	0.001152	0.71%	15.25	0.003
$f \times V$	1	0.000420	0.26%	5.57	0.040
$a \times V$	1	0.001104	0.68%	14.62	0.003
Error	10	0.000755	0.47%		
Lack-of-Fit	5	0.000755	0.47%		
Pure Error	5	0.000000	0.00%		
Total	19	0.162223	100.00%		

According to the ANOVA results, the vibration amplitude significantly affects the forming force and plastic strain, with contribution percentages of 90.89% and 82.41%, respectively. The punch speed affects both output parameters, while the resonant frequency affects only the plastic strain. In order to develop mathematical models for the forming force and plastic strain, the second-order regression analysis of the RSM was used. The regression model analysis was carried out using the Minitab statistical software. Ultimately, the parameters with significant contribution were identified from the results of the ANOVA test, and mathematical modeling coefficients for the output parameters of plastic strain and forming force were derived using Equations (1) and (2). The adjusted coefficient of determination (R^2-adjusted) in the regression models of forming force and plastic strain is 96.05% and 99.12%, respectively, while the R^2-predicted coefficients are 93.77% and 96.38%, indicating a good fit.

$$Forming\ Force = 17.870 - 0.4825a + 0.1540V + 0.00467a^2 \quad (1)$$

$$Plastic\ Strain = 3.851 - 0.3512f - 0.03542a + 0.0341V + 0.00875f^2 + 0.000558a^2 + 0.000642V^2 + 0.0016f \times a - 0.002071f \times V - 0.000448a \times V \quad (2)$$

3.2. Forming Force

The main effects plots of the input parameters on the forming force are presented in Figure 8. During the USSE process, it is of particular importance to reduce the friction between the sample and the die channel in order to reduce the forming force. As can be seen in Table 3, only the parameters of the vibration amplitude and punch speed have a significant effect on the forming force; the resonant frequency does not have a significant effect on this parameter. As shown in Figure 8, as the vibration amplitude is increased and transferred to the samples, the friction decreases, reducing the forming force incrementally. Moreover, as the punch speed decreases, the forming force decreases significantly, which can be explained by the fact that the lower the punch speed, the more time the sample is in contact with the vibrating horn and the die channel, and the more significant the reduction of the friction occurs in practice. According to Table 3, the interaction effects of the input parameters on the forming force are not significant. Acoustic softening in materials typically results from a combination of point, line, and planar defects, along with thermal effects. Each type of defect locally reduces the lattice's resistance to vibrations, ultimately giving rise to lower-frequency acoustic modes.

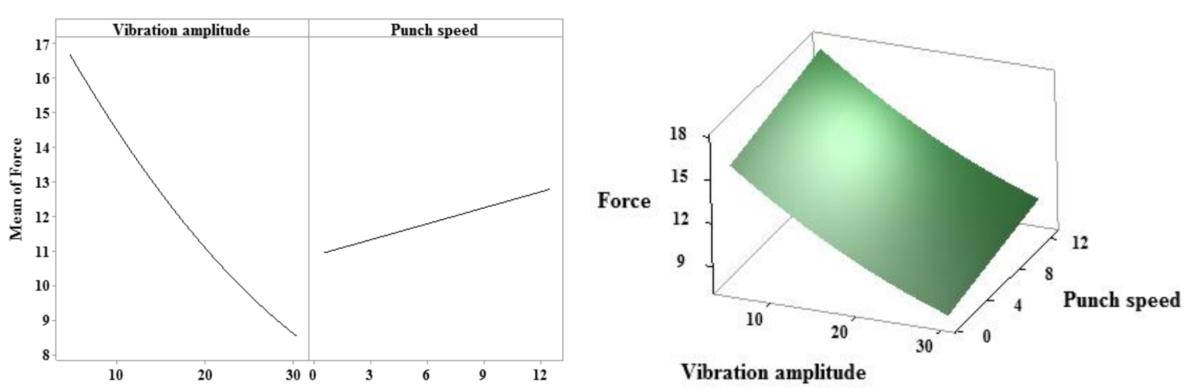

Figure 8. The effect of input parameters on forming force

3.3. Plastic Strain

The main and interaction effects of the input parameters on the plastic strain are presented in Figures 9 and 10, respectively. Increased plastic strain and uniform distribution of plastic strain in most SPD methods occur in the further passes, which is why the first pass of extrusion in the USSE process plays a significant role in increasing the plastic strain. As can be seen in Table 4, the values of vibration amplitude, punch speed, and resonant frequency have significant effects on plastic strain. According to Figure 9, as the resonant frequency and vibration amplitude increase, the plastic strain increases as well. In addition, as the punch speed decreases, the plastic strain increases. As can be seen in the interaction plots presented in Figure 10, the plastic strain increases as the resonant frequency increases and the punch speed decreases. Also, an increase in the vibration amplitude and a decrease in the punch speed lead to an increase in the plastic strain. As a result, the values leading to the highest plastic strain were recorded as follows: a vibration amplitude of 25 µm, a resonant frequency of 21 kHz, and a punch speed of 3 mm/min. Acoustic hardening refers to the phenomenon in which a material exhibits an increased mechanical resistance or apparent hardness when subjected to sound waves or vibrations. In other words, the material's response to rapid or cyclic loading is enhanced. Acoustic hardening occurs due to changes in the behavior of dislocations within the crystal structure of materials. Several key mechanisms are involved in this process. Sound waves cause the movement and slip of dislocations within the crystal lattice. When the number of dislocations increases or they become pinned in certain locations, their mobility is restricted, leading to an increase in the material's resistance to subsequent strains. Mobile dislocations can interact and form a tangled network. This network reduces the mobility of dislocations and, as a result, increases the hardness of the material. Dislocations generate their own local stress fields. When the material is subjected to vibrations, these stress fields interact with the stresses from the acoustic waves, making the movement of dislocations more difficult and leading to increased hardness. Acoustic waves usually operate at high frequencies, causing the material to behave under high strain rates. Under these conditions, dislocations do not have enough time to fully relax or move over long distances, making the material appear harder.

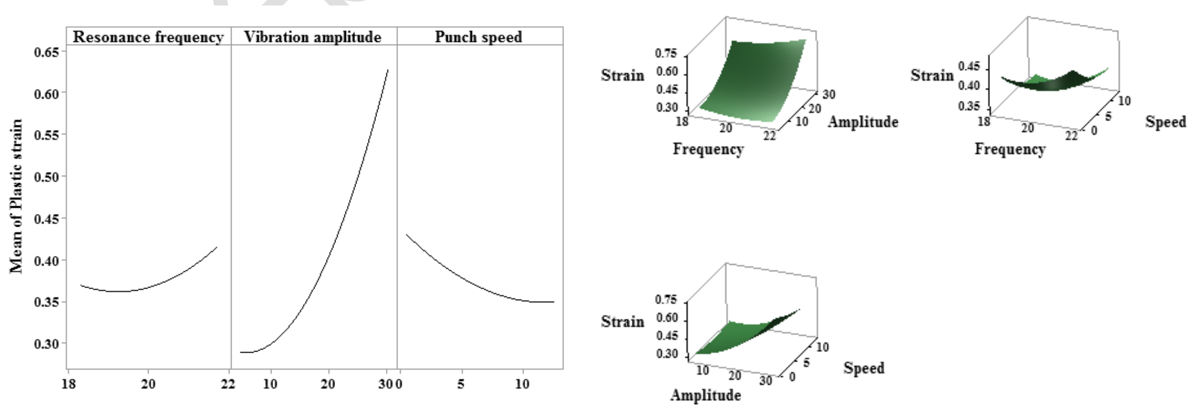

Figure 9. The main effect of input parameters on plastic strain

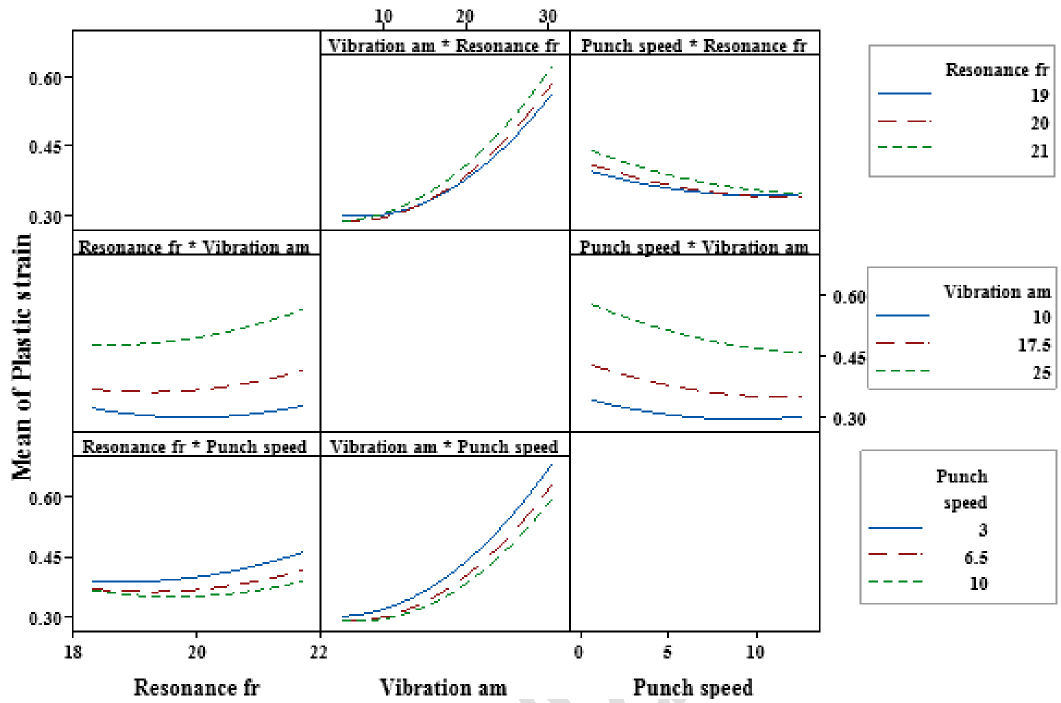

Figure 10. The interactions of input parameters on plastic strain

3.4. Optimization

Each parameter has different effects on the output parameters, i.e. plastic strain and forming force. Therefore, in order to find the optimal conditions to achieve the desired results, the USSE process was optimized using Response Optimizer in Minitab software. The multi-objective problem is associated with the maximum plastic strain and the minimum forming force. The criteria determined for the optimization of the output parameters, as well as the results of the optimal values, are shown in Figure 11. A vibration amplitude of 30.1134 µm, a punch speed of 0.6137 mm/min, and a resonant frequency value of 21.6818 kHz result in the maximum plastic strain and minimum forming force with a composite desirability of 1.

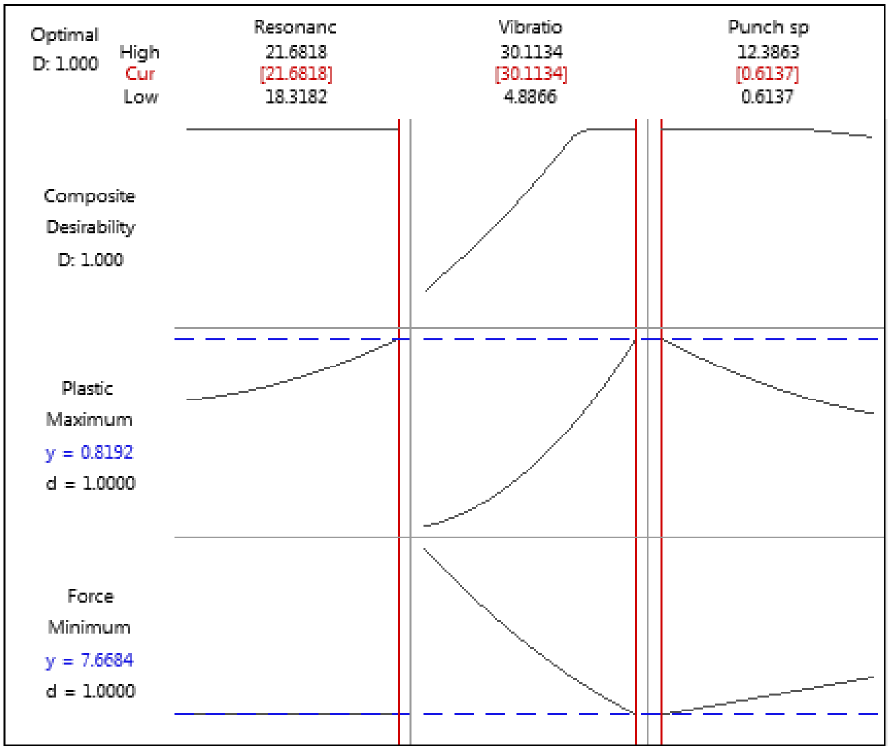

Figure 11. Graphical illustration of optimal results

The results from the FE simulation with the optimal values show a plastic strain value of 0.8812 and a forming force value of 7.9644 kN. A comparison between the results of the optimization output parameters (F=7.6684 kN, ε=0.8192) and the simulation (F=7.9644 kN, ε=0.8812) indicates a good and acceptable match with an error value of about 3% for the forming force and 7% for the plastic strain. After obtaining these optimal values from the experimental design, they were re-examined using experimental tests to compare optimal and non-optimal parameters. The optimal punch speed of 0.6137 mm/min could be directly entered into the data monitoring settings of the press machine, so that the mandrel performs the sample extrusion process at a low speed. To achieve the target vibration amplitude of 30.1134 μm, modifications to the horn's dimensions were implemented through modal analysis, and the generator output power was also changed.

3.5. Tensile Test

Several experiments were performed to produce the samples for tensile characteristics comparison, as Table 6. Also, the tensile properties of the annealed specimen were obtained. Experiment P_4 is the final specimen produced under optimized conditions.

Table. 6. Experimental setup for tensile characteristics comparisons

Experiment	*f* (kHz)	*a* (μm)	*V* (mm/min)
P_1 (SSD)	-	-	10
P_2 (USSD)	20	15	10
P_3 (USSD)	20	25	10
P_4 (USSD)	21.6818	30.1134	0.6137

The tensile test results for Experiments P_1, P_2, P_3, and P_4 are presented in Figure 12, which shows that the strength of the specimens produced by the USSE process is higher than that of the SSE process. At least three tensile specimens were tested for each processing condition to ensure statistical reliability. Engineering stress–strain curves were recorded, from which the yield strength, ultimate tensile strength (UTS), and elongation to failure were extracted. Deformation uniformity, fracture location, and failure mode were also examined and correlated with key USSE parameters (vibration amplitude, punch speed, and number of passes). This procedure enabled a clear assessment of the mechanical property enhancements resulting from ultrasonic assistance, particularly improvements in strength, ductility, and strain homogeneity. Specifically, operating the punch at very low speeds (<1 mm/min) considerably increases the forming time, leading to prolonged continuous ultrasonic vibration exposure. Under these conditions, the transducer–booster–horn assembly experiences elevated thermal loads, requiring extended cooling intervals to avoid depolarization of the piezoelectric elements and ensuring stable resonance tracking of the ultrasonic generator. These thermal, temporal, and stability constraints limited the number of feasible experiments at ultra-low punch speeds. Despite these limitations, the selected P4 condition was chosen carefully because preliminary trials indicated that it represented the most effective speed range for capturing the influence of low punch velocity on material flow, formability, and the resulting mechanical response. The purpose of including P4 was therefore to provide a representative point within the slow-speed domain rather than to conduct a full factorial expansion at this range. The observed improvements at P4 clearly highlight the significance of punch speed as an influential parameter. An increase in the material strength in the USSE method occurs due to the application of ultrasonic vibrations, so that the material strength increases as a result of an increase in the vibration amplitude. In the USSE method, the ultimate tensile strength (UTS) of specimen P_4 (the optimized condition) has increased by 6% and 2% compared to specimens P_2 and P_3, respectively. A comparison of the UTS between the first passes of P4 (USSE) and P1 (SSE) also showed an increase of 10%. In the USSE method, in addition to the vibration amplitude, which plays an effective role in improving the mechanical properties, the punch speed can also be mentioned as an effective parameter. The lower the punch speed, the longer the transmission of ultrasonic vibrations is in contact with the workpiece, and the more effective the role it plays in improving the mechanical properties. The UTS values derived in the first pass of the USSE method are close to those of the third and fourth passes in the SSE method, which confirms the high efficiency of this technique. This is also in accordance with the Hall-Petch equation (Equation 3), which denotes that the size of the grains has an inverse relationship with the yield strength, so that as the grains become smaller, the yield strength of the material increases [28].

$$\sigma_y = \sigma_0 + KD^{-\frac{1}{2}} \tag{3}$$

Where σ_y is the yield strength, *D* is the average diameter of the grains, σ_0 is the lattice friction (resistance to dislocation movement), and *K* is a material-specific constant.

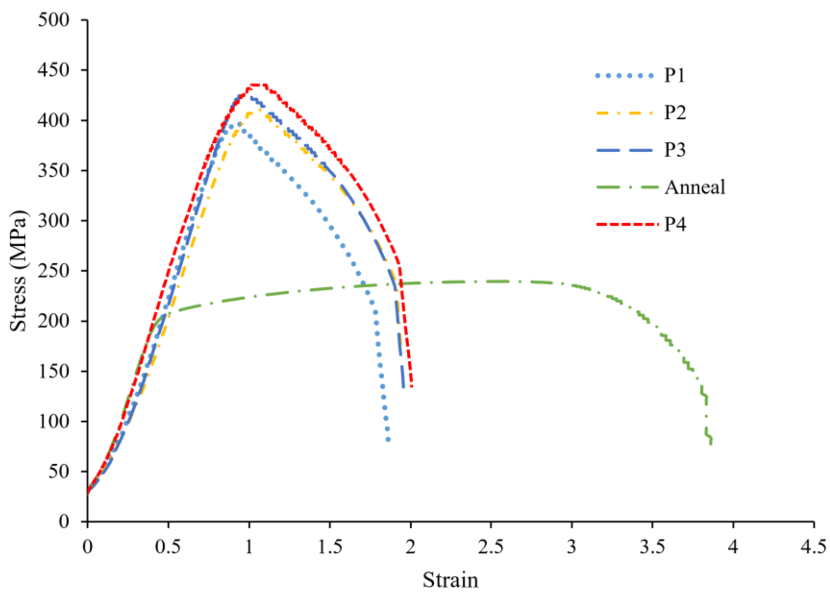

Figure 12. Stress-strain diagram in the SSE and USSE methods

Also, an increase in the yield strength as well as in the ultimate tensile strength can be explained by an increase in the dislocation density of the material structure, as expressed in Taylor Equation (4) [29].

$$\rho_{tot} = \left(\frac{\sigma_i}{M\alpha Gb}\right)^2 \tag{4}$$

where ρ_{tot} denotes the total dislocation density, σ_i is the flow stress, *M* is the Taylor factor, *G* is the shear modulus, α is a dimensionless geometric constant, and *b* is the magnitude of the Burgers vector. The increase in the material strength in the USSE process can be attributed to the formation of grain boundaries and the acoustic hardening that occurs after stopping the application of ultrasonic vibrations [30]. Acoustic hardening leads to a decrease in the material ductility and strain before reaching failure, which is due to the brittleness, fragility, and decreased twin formation [31]. The tensile properties of the material vary significantly with processing history, demonstrating a clear trade-off between strength and ductility, as summarized in Table 7. A consistent strengthening trend is observed from condition P1 to P4. Both yield strength (YS) and ultimate tensile strength (UTS) increase progressively, with P4 exhibiting the highest strength properties (YS: ~280 MPa, UTS: ~445 MPa). This progression suggests that the sequence from P1 to P4 represents increasing levels of work hardening or microstructural refinement induced by the respective processing routes. Concurrently, ductility, measured by total elongation, shows a more complex relationship. While elongation is lowest for P1 (~1.75%) and improves slightly through P2 (~1.90%) and P3 (~2.0%), it peaks markedly in the Annealed condition at ~3.8%. This substantial increase in elongation is accompanied by a pronounced drop in strength (YS: ~185 MPa, UTS: ~280 MPa), which is characteristic of the softened, recrystallized microstructure resulting from annealing. Condition P4, despite having the highest strength, maintains a reasonable ductility of ~2.3%, indicating a potentially favorable balance. In conclusion, the Annealed condition provides optimal ductility at the expense of strength, whereas the P-series conditions offer progressively higher strength with varying but lower ductility. The P4 condition appears to offer the most promising combination of high strength and moderate ductility among the non-annealed states. This inverse relationship between strength and elongation is a classic manifestation of the strength-ductility trade-off, and the specific properties are dictated by the microstructural state (e.g., dislocation density, grain size) produced by each processing method. These results effectively benchmark the mechanical performance window achievable through the studied processing routes.

Table. 7. values of tensile properties for different processing conditions (P1, P2, P3, Annealed, and P4)

Condition	Yield Strength (0.2% Offset) (MPa)	Ultimate Tensile Strength (MPa)	Total Elongation (%)
P1	~220	~390	~1.75
P2	~240	~410	~1.90
P3	~265	~425	~2
Anneal	~185	~280	~3.8
P4	~280	~445	~2.3

3.6. Surface Roughness

The R_a method was used in order to measure surface roughness. The measurement range of the samples and their results are shown in Figure 13. Surface roughness (R_a) was measured using a contact profilometer under controlled laboratory conditions. Measurements were performed along the extrusion direction over a length of 3 mm, with a cut-off length of 0.8 mm, and a measurement speed of 0.5 mm/s. For each sample, at least three measurements were taken at different locations on the extruded surface to ensure reproducibility. The surface roughness in the first pass of USSE samples (P_2, P_3, P_4) is less than that of the first pass of the SSE sample (P_1) and the annealed sample. The average surface roughness of Specimen P4 decreased by 21%, 9%, and 6% compared to that of P1, P2, and P3, respectively. Considering the application of almost identical strains on the surface of the USSE samples, the uniformity of the surface roughness values is higher compared to the SSE method, so that the most uniformity and homogeneity was reported in the optimal USSE process (P_4). By comparing the first pass of the SSE and USSE methods, it can be concluded that the two parameters of vibration amplitude and punch speed play a critical role in improving the surface roughness. In case of a simultaneous increase in amplitude and a decrease in punch speed, the efficiency of the USSE method is improved as well. The difference between the amplitudes of the workpiece and the die turns static friction into dynamic friction, leading to the elimination of the stick-slip motion, and this, in turn, helps better lubrication and material flow [32]. Due to the better lubrication in the USSE method, the friction between the die channel and the samples decreases more, which significantly contributes to the decreased surface roughness of the samples and subsequently their smoothness.

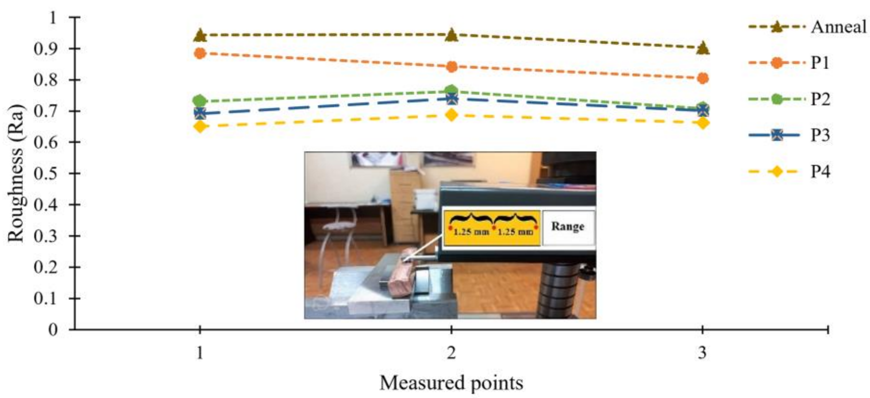

Figure 13. Roughness comparison in SSE and USSE specimens

For an accurate calculation of the standard deviation (SD) of surface roughness (R_a), individual measurements for each sample are required. The standard deviation is defined as:

$$SD = \sqrt{\frac{\sum_{i=1}^{N} (x_i - \bar{x})^2}{N-1}} \quad (5)$$

where x_i is each measured value, $\bar{x}$ is the mean of the measurements, and N is the number of measurements. Therefore, the average surface roughness (Ra) and its corresponding standard deviation were calculated based on the measured data points using Equation (5) (e.g., the standard formula for sample standard deviation). The results are summarized in Table 8.

Table. 8. Mean Surface Roughness (R_a) and Estimated Standard Deviation for SSE and USSE Samples

Sample	Mean R_a (µm)	Estimated SD (µm)
A	0.92	0.046
P1	0.86	0.043
P2	0.71	0.036
P3	0.69	0.035
P4	0.66	0.033

The surface roughness measurements indicate a clear improvement in the smoothness of samples processed by the USSE method compared to the conventional SSE and annealed samples. Sample A (annealed) exhibits the highest mean Ra (0.92 µm), reflecting the initial roughness before deformation. Among the processed samples, the SSE sample (P1) shows a slight reduction in roughness (0.86 µm), whereas the USSE samples (P2–P4) demonstrate a more substantial decrease, with mean Ra values of 0.71, 0.69, and 0.66 µm, respectively. This trend indicates that the combined effect of ultrasonic vibrations and optimized punch speed in the USSE process significantly enhances surface quality. Notably, sample P4, which corresponds to the optimal USSE condition, achieves the lowest roughness (0.66 µm) and the smallest estimated SD (0.033 µm), highlighting both improved smoothness and higher uniformity across the measured points.

3.7. Microstructure

The grain structure in the first pass of the optimal USSE method, i.e. Experiment P_4, is shown in Figure 14 compared to the annealed samples and the first pass of SSE (Experiment P_1). The grain structure in the annealed sample is coarse and homogeneous, with an average grain size of 142 µm. The image of the SSE sample shows that due to the application of different strains in the plastic deformation zone of the die, the distribution of grains is non-homogeneous with coarse and fine-sized grains next to each other, so that the average grain size was reported to be 23 µm. In most SPD methods, a high number of passes is needed to achieve a homogeneous equiaxed grain structure. This problem has been solved to a large extent by using the USSE method. In the USSE method, by applying ultrasonic vibrations to the samples, uniform strain is introduced throughout the sample, which further contributes to the homogenization of the microstructure. The average grain size in the first pass of the Specimen P_4 is 4 µm, which reports a 97% and 82% decrease in the grain size compared to the annealed sample and the SSE sample (P_1), respectively. The fineness of the structure can be expressed in the following way: By applying ultrasonic vibrations, the internal temperature of the samples increases, and this parameter has a significant effect on the movement and rotation of the grain boundaries. As a result, the rotation speed in the grain boundaries increases, and the fine-grain structure occurs faster. Dislocations mostly accumulate behind the grain boundaries, and as the vibration amplitude increases, the boundaries with a low angle are progressively transformed into the boundaries with a high angle, which leads to the fineness of the grains [33]. The USSE method with high vibration amplitude can be used to reach the nanostructure in fewer passes and a shorter time compared to the SSE process. In the reference specimen (Fig. 14(a)), the microstructure is composed of large, well-defined polygonal grains, with grain boundaries clearly visible at the 50 µm scale. Several grains exhibit elongated or partially columnar features, indicating solidification dominated by competitive dendritic growth. The overall morphology reflects a low nucleation rate and unrestricted grain growth, which results in coarse grains characteristic of solidification without external perturbation. With the introduction of ultrasonic vibration (Fig. 14(b)), the initially coarse grain morphology disappears, and the microstructure becomes noticeably more homogeneous and fine. Although individual grain boundaries are no longer well-resolved at this magnification due to their significantly reduced size, the surface texture shows a substantial increase in grain density and a clear suppression of coarse grain growth. This reflects a transition toward a nucleation-dominated microstructure, consistent with the onset of cavitation events and moderate dendrite fragmentation during solidification. Further refinement is achieved under a higher ultrasonic intensity (Fig. 14(c)), where the microstructure becomes extremely fine and uniformly distributed across the entire field of view. No large grains or elongated solidification features can be observed, and the texture indicates the formation of ultrafine equiaxed grains. The high uniformity implies that ultrasonic vibration has strongly disrupted dendritic growth, promoted extensive grain multiplication, and suppressed segregation-driven coarsening.

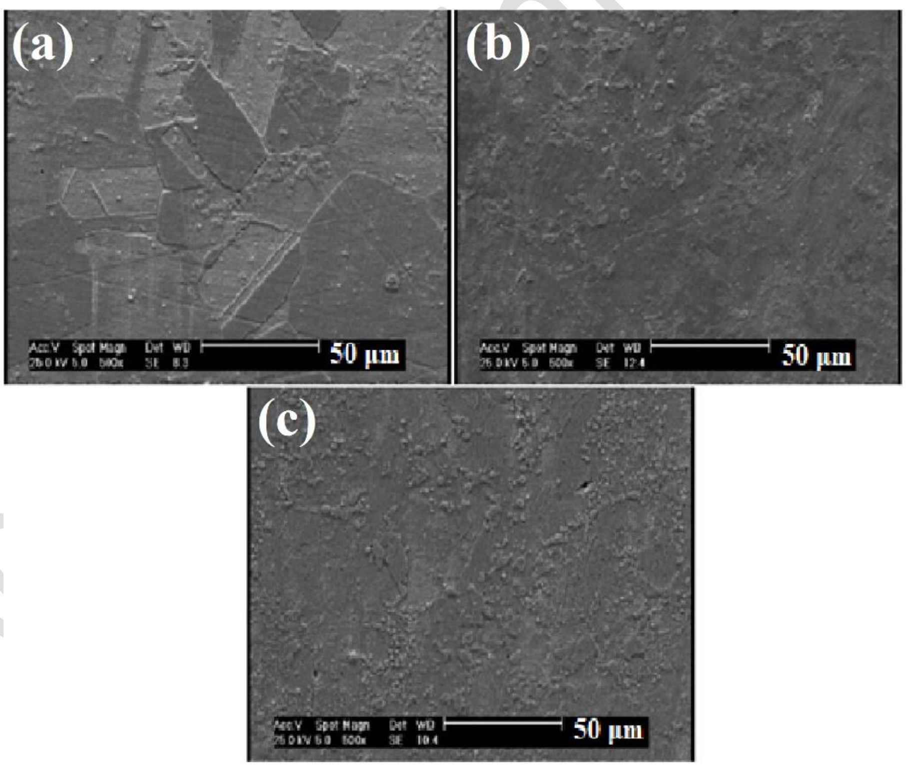

Figure 14. (a) SEM image of the annealed sample, (b) the first pass of the SSE sample (P_1), (c) the first pass of the USSE optimal sample (P_4)

5. Conclusion

This study investigated and optimized the ultrasonic-assisted simple shear extrusion (USSE) process for commercial pure copper using finite element analysis (FEA) combined with the Response Surface Method (RSM). Statistical modeling confirmed the significant influence of ultrasonic vibrations, identifying vibration amplitude as the most significant parameter for reducing forming force and increasing plastic strain. Increasing vibration amplitude and lowering punch speed markedly decreased friction and forming force due to longer contact between the sample and the vibrating horn.

The optimal USSE conditions 30.1134 μm vibration amplitude, 0.6137 mm/min punch speed, and 21.6818 kHz resonant frequency maximized plastic strain and minimized forming force. Under these conditions, ultimate tensile strength increased by 10% compared with conventional SSE, and a much finer, more homogeneous grain structure was produced. Average grain size decreased from 142 μm in the annealed state to 4 μm in the optimized USSE sample, a 97% reduction. Surface roughness also improved: the optimized USSE parameters reduced roughness by 9% and 6% compared with 15 and 25 μm amplitudes, and by 21% compared with SSE.

In summary, the USSE technique overcomes limitations of conventional SPD methods and provides an efficient route to materials with enhanced mechanical properties and refined, uniform microstructures in a single pass. The method shows strong industrial potential where superior properties with fewer processing steps are essential. While this study focused on pure copper, future work should examine alloy systems, industrial-scale implementation, and the quantification of thermal effects during ultrasonic processing.

References

[1] R. Z. Valiev and T. G. Langdon, “Principles of equal-channel angular pressing as a processing tool for grain refinement,” *Progress in Materials Science*, vol. 51, no. 7, pp. 881–981, 2006.

[2] D. Orlov, Y. Beygelzimer, S. Synkov, V. Varyukhin, N. Tsuji, and Z. Horita, "Plastic flow, structure and mechanical properties in pure Al deformed by twist extrusion," *Mater. Sci. Eng. A*, vol. 519, no. 1-2, pp. 105-111, 2009.

[3] C. Wang, F. Li, J. Liu, and J. Li, “Deformation analysis of elliptical cross-section spiral equal channel extrusion technique,” *Rare Metal Materials and Engineering*, vol. 42, no. 4, pp. 679–683, 2013.

[4] N. Pardis and R. Ebrahimi, "Deformation behavior in simple shear extrusion (SSE) as a new severe plastic deformation technique," *Materials Science and Engineering: A*, vol. 527, no. 1-2, pp. 355–360, 2009.

[5] C. Wang, F. Li, Q. Li, and L. Wang, "Numerical and experimental studies of pure copper processed by a new severe plastic deformation method," *Materials Science and Engineering: A*, vol. 548, pp. 19–26, 2012.

[6] Z. Huang, M. Lucas, and M. J. Adams, "Influence of ultrasonics on upsetting of a model paste," *Ultrasonics*, vol. 40, no. 1-8, pp. 43–48, 2002.

[7] B. Langenecker, "Effects of ultrasound on deformation characteristics of metals," *IEEE Transactions on Sonics and Ultrasonics*, vol. 13, no. 1, pp. 1–8, 1966.

[8] M. Zabihi, E. Emadoddin, and F. Qods, "Processing of Al/Al_2O_3 composite using simple shear extrusion (SSE) manufactured by Powder Metallurgy (PM)," *Metals and Materials International*, vol. 26, no. 1, pp. 1–13, 2019.

[9] F. Sayari, R. Roumina, R. Mahmudi, M. M. Hoseini-athar, and P. Hedström, "Comparison of the effect of ECAP and SSE on microstructure, texture, and mechanical properties of magnesium," *Journal of Alloys and Compounds*, vol. 908, p. 164407, 2022.

[10] A. Rezvani, E. Bagherpour, and R. Ebrahimi, "Circular simple shear extrusion as an alternative to simple shear extrusion technique," *Iranian Journal of Science and Technology, Transactions of Mechanical Engineering*, vol. 44, no. 1, pp. 193–201, 2018.

[11] E. Bagherpour, F. Qods, R. Ebrahimi, and H. Miyamoto, "Nanostructured pure copper fabricated by simple shear extrusion (SSE): A correlation between microstructure and tensile properties," *Materials Science and Engineering: A*, vol. 679, pp. 465–475, 2017.

[12] M. Balali, S. M. H. Seyedkashi, A. Hasanabadi, H. Gorji, H. Baseri and M. Khosravi, "Effects of Horn Type on the Microhardness and Microstructural Homogeneity in Ultrasonic-Assisted Simple Shear Extrusion," *Experimental Techniques*, vol. 49, no. 2, pp. 253-266, 2025.

[13] M. Balali, S. M. H. Seyedkashi, A. Hasanabadi, H. Gorji, H. Baseri and M. Khosravi, "A new ultrasonic-assisted simple shear extrusion process in production of ultrafine grained coppe". *International Journal of Engineering, Transactions A: Aspects*, vol. 38, no. 4, pp. 908-920, 2025.

[14] J. C. Hung and C. Hung, "The influence of Ultrasonic-vibration on hot upsetting of aluminum alloy," *Ultrasonics*, vol. 43, no. 8, pp. 692–698, 2005.

[15] M. Balali, S. M. H. Seyedkashi, A. Hasanabadi, H. Gorji, H. Baseri and M. Khosravi, "Optimization of effective parameters on ultrasonic horns in simple shear extrusion process using Taguchi design of experiments," *Iranian Journal of Manufacturing Engineering*, vol. 11, no. 3, 1-12, 2024. (In Persian)

[16] X. Wang and Y. Yu, "Experimental investigation on GCR15 Steel for marine vessels treated by ultrasonic-assisted equal channel angular extrusion," *Journal of Coastal Research*, vol. 83, no. sp1, p. 548, 2019.

[17] S. Bagherzadeh, K. Abrinia, and Q. Han, "Analysis of plastic deformation behavior of ultrafine-grained aluminum processed by the newly developed ultrasonic vibration enhanced ECAP: Simulation and experiments," *Journal of Manufacturing Processes*, vol. 50, pp. 485–497, 2020.

[18] A. P. Zhilyaev, A. A. Samigullina, A. E. Medvedeva, S. N. Sergeev, J. M. Cabrera, and A. A. Nazarov, "Softening and hardening of ECAP nickel under ultrasonic treatment," *Materials Science and Engineering: A*, vol. 698, pp. 136–142, 2017.

[19] M. Rasooli, M. Moshref-javadi, and A. Taherizadeh, "Investigation of ultrasonic vibration effects on the microstructure and hardness of aluminum alloy 2024 tube spinning parts," *The International Journal of Advanced Manufacturing Technology*, vol. 77, no. 9-12, pp. 2117–2124, 2014.

[20] Z. Xie, F. Chen, and W. He, "The effects of ultrasonic vibration on riveting quality," *Scientific Reports*, vol. 12, no. 1, 2022.

[21] A. N. Ali and S. J. Huang, "Ductile fracture behavior of ECAP deformed az61 magnesium alloy based on response surface methodology and finite element simulation," *Materials Science and Engineering: A*, vol. 746, pp. 197–210, 2019.

[22] A. I. Alateyah *et al.*, "Optimizing the ECAP processing parameters of pure CU through experimental, finite element, and response surface approaches," *Reviews on Advanced Materials Science*, vol. 62, no. 1, 2023. 0297

[23] G. Ranjbari, A. Doniavi, and M. Shahbaz, "Numerical modelling and simulation of vortex extrusion as a severe plastic deformation technique using response surface methodology and finite element analysis," *Metals and Materials International*, vol. 27, no. 8, pp. 2898–2909, 2020.

[24] U. Mohammed Iqbal, V. S. Senthil Kumar, and S. Gopalakannan, "Application of response surface methodology in optimizing the process parameters of twist extrusion process for AA6061-T6 Aluminum Alloy," *Measurement*, vol. 94, pp. 126–138, 2016.

[25] W. Littmann, H. Storck, and J. Wallaschek, “Sliding friction in the presence of ultrasonic oscillations: Superposition of longitudinal oscillations,” *Archive of Applied Mechanics (Ingenieur Archiv)*, vol. 71, no. 8, pp. 549–554, 2001.

[26] F. Djavanroodi, H. Ahmadian, R. Naseri, K. Koohkan, and M. Ebrahimi, “Experimental investigation of ultrasonic-assisted equal channel angular pressing process,” *Archives of Civil and Mechanical Engineering*, vol. 16, no. 3, pp. 249–255, 2016.

[27] O. Mehrabi, S. M. H. Seyedkashi, M. Moradi, Experimental and response surface study on additive manufacturing of functionally graded steel-Inconel wall using direct laser metal deposition, *Optics and Laser Technology*, vol. 167, 109707, 2023.

[28] O. Mehrabi, S. M. H. Seyedkashi, and M. Moradi, “Effect of the scanning strategy in the laser directed energy deposition process of SS316L-Inconel 625 FGM bulk,” *The International Journal of Advanced Manufacturing Technology*, vol. 135, no. 11-12, pp. 5747–5761, 2024.

[29] J. C. Hung and C. C. Lin, “Investigations on the material property changes of ultrasonic-vibration assisted aluminum alloy upsetting,” *Materials & Design*, vol. 45, pp. 412–420, 2013.

[30] E. A. El-Danaf, “Mechanical properties and microstructure evolution of 1050 aluminum severely deformed by ECAP to 16 passes,” *Materials Science and Engineering: A*, vol. 487, no. 1-2, pp. 189–200, 2008.

[31] T. Wen, L. Wei, X. Chen, and C. Pei, “Effects of ultrasonic vibration on plastic deformation of AZ31 during the tensile process,” *International Journal of Minerals, Metallurgy, and Materials*, vol. 18, no. 1, pp. 70–76, 2011.

[32] G. Ngaile, and C. Bunget” Influence of Ultrasonic Vibration on Microforming,” *Transactions of NAMRI,* 36, pp. 137-143, 2008.

[33] J. C. Hung and C. C. Lin, “Investigations on the material property changes of Ultrasonic-vibration assisted aluminum alloy upsetting,” *Materials & Design*, vol. 45, pp. 412–420, 2013.